Theor Chem Acc (1998) 99:166–170

Theoretical
Chemistry Accounts

Regular article

Density functional calculations of the pseudorotational flexibility of tetrahydrofuran

Marek Štrajbl[1], **Jan Florián**[2]

[1] Institute of Physics, Charles University, Ke Karlovu 5, CZ-121 16 Prague 2, Czech Republic
[2] Department of Chemistry, University of Southern California, Los Angeles, CA 90089-1062, USA

Received: 17 June 1997 / Accepted: 20 November 1997

Abstract. The flexibility of the five-membered ring in tetrahydrofuran was investigated using quantum mechanical methods involving density functional, Hartree-Fock, and many-body perturbation theory (MP2, MP4) calculations. We found that motion along the pseudorotational path of tetrahydrofuran is nearly free. The 0.1 kcal/mol energy barrier for pseudorotation, calculated at the highest MP4(SDQ)/6-311++G(2*d*,*p*)//MP2/6-311++G(2*d*,*p*) level of theory, agrees well with the experimental value of 0.16 ± 0.03 kcal/mol. Similar results were obtained with the S-VWN, B3-LYP and B-LYP density functional calculations using the 6-31G(*d*) set of atomic orbitals. Also the density functional dipole moments and geometries were in good agreement with both the MP2 and experimental benchmarks. However, all density functional methods that utilized the default integration grid in the Gaussian 94 program were found to provide false stationary points of the C_1 symmetry near the pseudorotational angle of 100°. These stationary points disappeared when a denser spherical-product grid was used. Overall, the hybrid B3-LYP functional was found to be the most promising quantum mechanical method for the modeling of biomolecules containing the furanose ring.

Key words: Tetrahydrofuran – Pseudorotation – Density functional theory – Ab initio calculations – Conformational analysis

1 Introduction

The recent introduction of density functional theory (DFT) algorithms that scale linearly with the size of the system [1–6] has opened new horizons in the application of rigorous quantum chemical methods in structural biochemistry. However, in contrast to the conventional ab initio calculations, whose accuracy can be systematically improved by increasing the number of basis functions and including higher levels of electron correlation treatment, the performance of different DFT functionals varies with the nature of the system studied. Therefore, the choice of the DFT method is usually not straightforward and must be based on the benchmark studies of smaller model systems. Because accurate description of weak intermolecular interactions and rotational barriers is essential in proteins and nucleic acids, performance of density functional methods in reproducing these properties needs to be critically evaluated. However, whereas hydrogen-bonding interactions [7–13] and rotations around amide bonds [14–16] have been thoroughly investigated at the DFT level, little attention has been paid to the conformational flexibility of the riboso-phosphate backbone of nucleic acids. To fill this gap we recently calculated B3-LYP/6-31G* torsional barriers of the phosphodiester bonds in dimethyl phosphate [17]. In the present work, we investigate the structure of the furanose ring in tetrahydrofuran (THF) by using the S-VWN, B-LYP and B3-LYP functionals as representatives of local, nonlocal and hybrid density functionals, respectively. The results of these calculations are compared with the barrier to the pseudorotation, dipole moment, and geometry of THF determined by microwave [18] and X-ray [19] spectroscopy. In addition, ab initio calculations involving Hartree-Fock (HF), Møller-Plesset perturbation theory of the second (MP2) and fourth (MP4) order are presented, and the important issue of the stability of the DFT results with respect to the numerical grid is addressed.

The furanose ring is the structural unit of nucleic acids and its puckering affects DNA structure and interactions to a large extent. As such, it has been subject of numerous experimental and theoretical investigations. An extensive survey of the available X-ray, spectroscopic, and computational data as well as original ab initio calculations was published by Cadioli et al. [20, 21]. The twisted conformation possessing C_2 symmetry was observed by X-ray structure analysis [19] and by high-resolution neutron powder diffraction [22] of THF in solid state. The same conformation was obtained at

Correspondence to: J. Florián, or M. Štrajbl

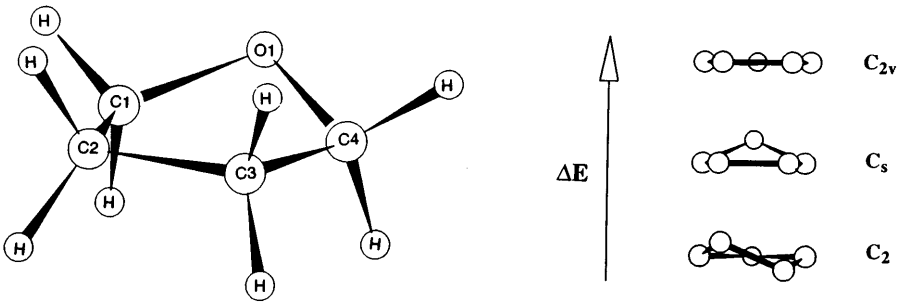

Fig. 1. Structure and atom numbering of various conformers of tetrahydrofuran

the HF and correlated (MP2/6-31G*) levels of theory as the global minimum on the gas phase potential energy surface [20, 21]. In this conformer, C2 and C3 atoms are displaced by equal amounts in the opposite directions from the C1OC4 plane (Fig. 1). Thus, the two symmetrically equivalent C_2-symmetry minima are classified as C2-endo and C3-endo, or, in the pseudorotation notation [23], as S- and N-conformers. Interestingly, these two conformers are also dominant forms of furanose sugars observed in X-ray structures of ribonucleotides [23, 24]. The transition between the C2-endo and C3-endo forms of the furanose ring can lead either via the planar structure possessing the C_{2v} symmetry, or along the pseudorotational path in which the positive displacement from the mean plane of the ring travels around the ring in the C2-endo → C1-endo → O-endo → C4-endo → C3-endo sequence. It turns out that the pseudorotational pathway is preferred for both THF [20, 21] and ribose [24, 25], although this is not always the case in other five-membered rings [26]. The transition state on the pseudorotational pathway may correspond either to the puckered structure of the C_s symmetry (envelope form) or it may possess no symmetry (C_1). In the latter case, the envelope form (C_s) would correspond to the local minimum of the pseudorotational potential.

2 Methods

Ab initio optimizations of geometric structure and computations of harmonic force fields were carried out with the Gaussian 94 [27] program. The HF, DFT, and MP2 as well as MP4(SDQ) perturbation theory with the standard 6-31G(*d*), 6-31+G(*d*,*p*), 6311+G(*d*,*p*), and 6-311++G(2*d*,*p*) polarized split-valence basis sets were used for these calculations. Frozen-core approximation, which includes only the valence electrons' contribution to the correlation energy, was used for the MP2 and MP4 calculations. Two types of exchange-correlation functionals were considered in the DFT calculations. These involve the local S-VWN [28] functional, and a combination of the nonlocal Becke's exchange functional [29] and the Lee-Yang-Parr correlation functional [30] (B-LYP). In addition, we employed the hybrid B3-LYP functional [31], which consists of a linear combination of HF and nonlocal density functionals. The sensitivity of DFT results with respect to the density of the grid for the numerical integral calculations was evaluated by using several grid types. These included the pruned (50,194) and (75,302) grids, which are usually referred to as the "standard" SG-1 [27, 32] and "fine" [27] grid, respectively. Here, the (N^r, N^Ω) notation lists the number of radial (N^r) and angular (N^Ω) grid points [32]. In addition, larger (90,302) and (75,434) grids were used to study separately the numerical consequences of the variations in the number of the radial and angular grid points. Finally, the benchmark (96,32,64) spherical product grid [33], which has 96 radial shells around each atom and 32×64 angular points in each shell, was used. The (75,302) grid is the default grid in the Gaussian 94 program [27].

The torsional flexibility of the five-membered furanose ring was described in terms of the phase angle of pseudorotation, P, and the degree of pucker, θ_m [23]. The relationships

$$\tan(P) = (\theta_2 + \theta_4 - \theta_1 - \theta_3)/2\theta_0(\sin(36^\circ) + \sin(72^\circ)), \quad (1)$$

and,

$$\theta_m^2 = 0.4 \sum \theta_j^2, \quad (2)$$

where the symbols θ_0, θ_1, θ_2, θ_3 and θ_4 denote torsional angles round the C2-C3, C3-C4, C4-O4, O4-C1 and C1-C2 bonds, respectively, were employed.

3 Results and discussion

The pseudorotational flexibility of THF was examined by comparing total energies and enthalpies at 0°K for the stationary points of the C_2, C_s, and C_{2v} symmetry (Table 1). Search for additional stationary points without any symmetry constraint (i.e. possessing C_1 symmetry) was carried out at the DFT level of theory because some DFT calculations yielded only positive vibrational frequencies for the C_s structure ($P = 90^\circ$ or 270°). This finding indicated that the transition state for the pseudorotation should possess no symmetry at the DFT level. Indeed, by using the S-VWN, B-LYP and B3-LYP functionals with the 6-31G* basis set and the default (75,302) grid spacing, these stationary points were located at P equal to 101.6, 103.1, and 95.3°, respectively. However, the relative energy of these nonsymmetric transition states was only by 0.01 kcal/mol larger than the energy of the corresponding C_s conformers. Moreover, the relative B-LYP energy of the C_s conformer was negative (−0.05 kcal/mol), and the extent of this energy reversal was further magnified when the larger 6-31+G** basis set was used. Because of the qualitatively different behavior of the DFT methods (as compared to the HF and MP2 methods) we checked the grid and basis set dependence of the DFT results (Table 1). First, we verified that the spurious C_1 stationary point does not disappear upon increasing the number of basis functions or radial grid points. On the other hand, we found that the energy of this conformer becomes lower than or equal to the energy of the C_s conformer when the (75,434) grid with a larger number of angular grid points was used. To confirm this finding we further increased the number of angular grid points by using the benchmark (96,32,64) grid. This

Table 1 Relative energy and enthalpy (kcal/mol) of different conformers of tetrahydrofuran (THF)[a]

Method	C_1		C_s		C_{2v}
	ΔE	ΔH_0[b]	ΔE	ΔH_0[b]	ΔH_0[b]
HF/6-31G*	n.s.p.[c]		0.39	0.45	3.3
SVWN/6-31G*					
SG1Grid	0.13	0.20	0.09	0.36	4.7
75,302	0.17	0.22	0.16	0.30	4.6
75,434	0.12	0.26	0.12	0.29	4.6
90,302	0.17	0.22	0.16	0.30	4.6
96,32,64	0.12	0.27	0.12	0.25	4.6
SVWN/6-31+G**					
SG1Grid	0.06	0.11	−0.01	0.28	4.5
75,302	0.07	0.20	0.06	0.23	4.4
75,434	n.s.p.[c]		0.02	0.21	4.4
90,302	0.07	0.17	0.06	0.21	4.4
96,32,64	n.s.p.[c]		0.02	0.19	4.4
SVWN/6-311+G**					
SG1Grid	0.07	0.22	0.03	0.28	4.5
75,302	0.09	0.14	0.07	0.22	4.5
75,434	n.s.p.[c]		0.03	0.21	4.4
90,302	0.09	0.18	0.07	0.24	4.5
96,32,64	n.s.p.[c]		0.03	0.19	4.4
B3LYP/6-31G*					
SG1Grid	0.11	0.21	0.05	0.30	3.3
75,302	0.13	0.21	0.12	0.25	3.3
75,434			0.10	0.21	3.2
90,302	0.13	0.20	0.11	0.24	3.2
96,32,64	n.s.p.[c]		0.10	0.21	3.2
B3LYP/6-31+G**					
75,302	0.05	0.19	0.04	0.20	3.2
B3LYP/6-311+G**					
SG1Grid	0.04	0.14	0.00	0.20	3.1
75,302	0.05	0.17	0.04	0.19	3.1
75,434	0.02	0.14	0.04	0.18	3.1
90,302	0.05	0.14	0.04	0.18	3.1
BLYP/6-31G*					
75,302	−0.02	0.11	−0.02	0.17	3.2
96,32,64	n.s.p.[c]		−0.05		3.2
BLYP/6-31+G**					
75,302	n.s.p.[c]		−0.11	0.09	3.1
MP2/6-31+G**	n.s.p.[c]		0.32	0.30	4.5
MP2/6-311++G(2d,p)	n.s.p.[c]		0.17		4.3
MP4/6-311++G(2d,p)[c]	n.s.p.[c]		0.08		3.7
exp[e]				0.16 ± 0.03	3.5 ± 0.1

[a] The energy and enthalpy at 0 K of the C_2 conformer was taken as the reference point
[b] $\Delta H_0 = \Delta E + \Delta ZPE$, where ΔZPE is the difference in the zero-point vibraional energy. ΔZPE of the C_{2v} conformers amounts to −0.1 kcal/mol for all methods
[c] Not a stationary point
[d] MP4(SDQ) energies were evaluated at the MP2/6-311++G(2*d*,*p*) geometries of stationary points
[e] The barrier heights to the pseudorotation, and the inversion via the planar configuration as determined from the microwave spectrum of THF [18]

spherical grid was found to result in 10^{-7} hartree (10^{-4} kcal/mol) accuracy for benzene [34]. Here, the spurious stationary point disappeared or its energy and geometry were within the numerical accuracy of the geometry optimizer identical to the C_s conformer. The S-VWN/6-31G*/(96,32,64) and B3-LYP/6-31G*/(96,32,64) vibrational frequency calculations carried out for the C_s conformer resulted in one imaginary frequency, confirming this conformer to be a transition state for the pseudorotation of THF. Since the CPU time needed for the B-LYP frequency calculations on the (96,32,64) grid is about 40 times longer than for the default (75,302) grid, we did not evaluate the B-LYP/(96,32,64) vibrational frequencies for the C_s conformer. Nevertheless, the reversal of the energies of the C_2 and C_s conformers ($P = 0°$ and 90°) seems to be the property of the B-LYP functional, as it is unchanged by the grid size. Furthermore, the identification of the C_2 structure as a transition state at the B-LYP level was confirmed by the calculated B-LYP/6-31G*/(96,32,64) vibrational frequencies of this conformer. In contrast, other computational methods put this conformer in the global minimum of the potential energy surface.

Although a small energy difference of the C_2 and C_s conformers of THF is not optimal for the assessment of the performance of ab initio methods, THF is unique in that its gas-phase pseudorotational barrier has been determined by microwave spectroscopy [18]. On the other hand, there are no reliable gas-phase experimental data available for the pseudorotational barrier in larger furanose-ring-containing molecules such as ribose and deoxyribose. The comparison of the calculated and experimental pseudorotational barriers must involve change in the zero-point vibrational energy (ΔZPE). Interestingly, the ΔZPE values tend to compensate for the electronic energy differences so that the resulting ΔH_0 values generally compare well with the corresponding experimental value of 0.16 kcal/mol (Table 1). This is true even for the B-LYP functional. To obtain a benchmark for the electronic energy differences we carried out the MP4 calculations in an extended basis set (Table 1). Considering the MP4 energies as well as the

experimental values of ΔH_0 for both the C_s and C_{2v} conformers, one can conclude that the hybrid B3-LYP functional shows the best overall results. This good performance, which is obtained even for the relatively small SG-1 grid and 6-31G* basis sets, chiefly results from the cancellation of errors between the HF exchange and B-LYP exchange-correlation functionals that are components of the B3-LYP hybrid. A relatively small basis set dependence of the B3-LYP results contrasts with the large basis set requirements of the MP2 method. The barrier to pseudorotation was also correctly predicted by the local S-VWN functional. On the other hand, this method significantly overestimated the barrier to planarization of the five-membered ring.

Because an accurate description of the electrostatic properties is important in biomolecular modeling, we evaluated the method dependence of the electrostatic dipole moment of THF (Table 2). At the highest MP2/TZP level, the magnitude of the dipole moment for the C_2 conformer is 1.94 Debye, whereas a dipole moment of 1.75 Debye was obtained experimentally [18]. The dipole size decreases by about 10% for the envelope (C_s) form of THF. A similar trend was obtained previously from microwave spectra [18], which provided values of about 1.6 Debye for excited pseudorotational states (lying above the pseudorotational barrier). This finding indicates that the global minimum of the gas phase potential energy surface of THF will be further stabilized in a polar environment. This trend was recently confirmed by using vibrational spectroscopy and the Langerin dipoles solvation model [35]. The ratio of the dipole moments of the C_2 and C_s conformers is reliably reproduced by all computational methods examined by us. As far as absolute accuracy is concerned, DFT methods with the 6-31G* basis set provide the best results.

Table 2. Dipole moment (Debye) of different conformers of THF

Method[a]	C_2	C_s	C_{2v}
HF/6-31G*	1.94	1.77	1.95
SVWN/6-31G*	1.73	1.48	1.78
SVWN/6-31+G**	1.96	1.70	1.98
SVWN/6-311+G**	1.94	1.69	1.97
BLYP/6-31G*	1.73	1.51	1.77
BLYP/6-31+G**	2.00	1.77	2.00
B3LYP/6-31G*	1.79	1.59	1.82
B3LYP/6-31+G**	2.01	1.81	2.02
B3LYP/6-311+G**	2.00	1.80	2.01
MP2/6-31+G**	2.10	1.88	2.10
MP2/6-311++G(*2d, p*)	1.94	1.74	1.92
exp[b]	1.75 ± 0.02		

[a] Results calculated by using the (75,302) grid are presented for DFT methods. Computations with different grids resulted in the same magnitudes of dipole moments
[b] Dipole moment observed for the ground vibrational state of THF via the Starck effect in the pure rotational spectrum [18]

The calculated geometry of the C_2, C_s and C_{2v} conformers of THF is given in Tables 3 and 4. We found all computational methods considered to yield reasonable agreement with the experimental results and that the basis set dependence of calculated results is quite small. More specifically, the use of the 6-31G(*d*) basis set resulted in shortening the CO bonds by about 0.006 Å compared to the bond lengths obtained with the larger 6-31 + G(*d,p*) basis set, whereas other parameters were practically unaffected by this basis set variation. In addition, differences smaller than 0.003 Å were found between the MP2/6-31+G(*d,p*) and MP2/6-311++G (2*d,p*) geometries. Comparison of the calculated and experimental values of θ_m indicates that THF as depicted by the MP2 and S-VWN methods is slightly more puckered than in crystal. The HF, B-LYP and B3-LYP methods predict a flatter geometry, which approximates X-ray data more closely. Overall, the B3-LYP/6-31 + G** method provides a geometry that agrees best with the observed crystal structure.

The degree of pucker, θ_m, is predicted to increase by about 4° for the envelope form (C_s) of THF. Because this change is relatively small, empirical models of THF pseudorotation that assume a constant θ_m for the whole pseudorotation cycle seem to be quite reasonable. In addition, there is notable coupling between the pseudorotational angle (*P*) and the C1OC4 bond angle (cf. Tables 3 and 4). This coupling as well as other geometry variations between the C_2, C_s and C_{2v} stationary points

Table 3. Calculated and experimental geometry of the C_2 conformation of THF

Pararameter[a]	HF	S-VWN[b]	B-LYP[b]	B3-LYP[b]	MP2	Experimental[d]	
	6-31G*		6-31+G**		TZP[c]	−170°	−125°
O1C1	1.409	1.419	1.458	1.437	1.439	1.429	1.435
C1C2	1.528	1.515	1.545	1.534	1.524	1.519	1.521
C2C3	1.529	1.518	1.550	1.537	1.529	1.504	1.541
C4O1C1	111.3	109.7	109.6	110.1	109.2	108.3	109.7
O1C1C2	106.1	106.0	106.4	106.2	106.0	107.4	106.8
C1C2C3	101.4	101.0	101.9	101.7	101.2	102.0	101.9
O1C1C2C3	30.4	33.0	30.6	30.6	33.0	29.7	29.6
C1C2C3C4	−36.0	−39.2	−36.4	−36.4	−39.3	−34.9	−35.2
θ_m	37.1	40.2	37.3	37.3	40.2	36.0	36.1

[a] For atom numbering see Fig. 1. Bond lengths and angles are given in Å and degrees, respectively. Only the geometry of symmetrically unique coordinates is presented
[b] The presented geometrical parameters were obtained by using the default (75,302) grid. Grid-related geometrical changes are smaller than 0.001 Å or 0.1°.
[c] 6-311 + + G(2*d,p*)
[d] X-ray structure for two different sample temperatures (°C) [19]

Table 4. Calculated geometry of the C_s and C_{2v} conformers of THF

Parameter[a]	HF	S-VWN[b]	B-LYP[b]	B3-LYP[b]	MP2
	6-31G*		6-31 + G**		TZP[c]
C_s geometry					
O1C1	1.401	1.409	1.447	1.428	1.428
C1C2	1.537	1.527	1.555	1.544	1.535
C2C3	1.546	1.538	1.569	1.555	1.549
C4O1C1	107.0	104.4	105.2	105.7	104.2
O1C1C2	105.5	105.4	105.6	105.6	105.4
C1C2C3	103.3	103.0	103.6	103.5	103.3
O1C1C2C3	−22.7	−25.1	−23.6	−23.4	−25.1
C1C2C3C4	0.0	0.0	0.0	0.0	0.0
θ_m	40.52	44.07	41.39	41.30	43.9
C_{2v} geometry					
O1C1	1.403	1.411	1.449	1.430	1.430
C1C2	1.539	1.529	1.556	1.545	1.537
C2C3	1.540	1.530	1.561	1.549	1.542
C4O1C1	113.4	112.3	111.8	112.3	111.8
O1C1C2	108.1	108.4	108.5	108.3	108.5
C1C2C3	105.2	105.4	105.6	105.5	105.6

[a] For atom numbering see Fig. 1. Bond lengths and angles are given in Å and degrees, respectively. Only the geometry of symmetrically unique coordinates is presented
[b] The presented geometrical parameters were obtained by using the default (75,302) grid. Grid-related geometrical changes are smaller than 0.001Å or 0.1°
[c] 6-311++G(2*d*,*p*)

are consistently described by both DFT and MP2 methods.

In conclusion, all structural properties of THF are reasonably well reproduced by the DFT methods examined in this work. However, the numerical instability with respect to the grid quadrature needs to be considered in DFT calculations of flexible systems. In the case of the pseudorotational barrier of THF, numerical errors related to the use of the SG1, (75,302), (75,434) and (96,32,64) grids can be estimated as 0.1, 0.05, 0.03, and <0.01 kcal/mol, respectively. These numerical errors are small compared to the differences between the experimental and calculated pseudorotational barriers of THF, but they will inevitably increase for larger molecules.

Acknowledgements. This work was supported by the Grant Agency of the Czech Republic (grant no. 203/93/2362). The calculations were carried out at the Supercomputing Center of Charles University and at the Joint Supercomputing Center of the Czech Technical University and the University of Chemical Technology. The kind help of Prof. Ivan Barvik is gratefully acknowledged.

References

1. Yang WT (1991) Phys Rev Lett 66:1438
2. Yang WT (1992) J Mol Struct (Theochem) 87:461
3. White CA, Johnson BG, Gill PMW, Head-Gordon M (1994) Chem Phys Lett 230:8
4. White CA, Johnson BG, Gill PMW, Head-Gordon M (1996) Chem Phys Lett 253:268
5. Hernandez E, Gillan MJ, Goringe CM (1996) Phys Rev B 53:7147
6. Strain MC, Scuseira GE, Frisch MJ (1996) Science 271:51
7. Sim F, StAmant A, Papai I, Salahub D (1992) J Am Chem Soc 114:4391
8. Kieninger M, Suhai S (1994) Int J Quantum Chem 52:465
9. Topol IA, Burt SK, Rashin AA (1995) Chem Phys Lett 247:112
10. Florián J, Johnson BG (1995) J Phys Chem 99:5899
11. Hobza P, Sponer J, Reschel T (1995) J Comput Chem 16:1315
12. Sponer J, Leszczynski J, Hobza P (1996) J Phys Chem 100:1965
13. Sponer J, Leszczynski J, Hobza P (1996) J Comput Chem 17:841
14. Barone V, Adamo C, Lelj F (1995) J Chem Phys 102:364
15. Oie T, Topol IA, Burt SK (1995) J Phys Chem 99:905
16. Kieninger M, Suhai S (1996) J Mol Struct 375:181
17. Florián J, Baumruk V, Strajbl M, Bednárová L, Stepánek J (1995) J Phys Chem 100:1559
18. Engerholm GG, Luntz AC, Gwinn WD, Harris DO (1969) J Chem Phys 50:2446
19. Luger P, Buschmann J (1983) Angew Chem 95:423
20. Cadioli B, Gallinella E, Coulombeau C, Jobic HGB (1993) J Phys Chem 97:7844
21. Gallinella E, Cadioli B, Flament JP, Berthier G (1994) J Mol Struct 315:137
22. David WIF, Ibberson RM (1992) Acta Crystallogr C 48:301
23. Altona C, Sundaralingam M (1972) J Am Chem Soc 94:8205
24. Olson WK, Sussman JL (1982) J Am Chem Soc 104:270
25. Levitt M, Warshel A (1977) J Am Chem Soc 100:2607
26. Cremer D, Pople JA (1975) J Am Chem Soc 97:1358
27. Frisch MJ, Trucks GW, Schlegel HB, Gill PMW, Johnson BG, Robb MA, Cheeseman JR, Keith T, Petersson GA, Montgomery JA, Raghavachari K, Al-Laham MA, Zakrzewski VG, Ortiz JV, Foresman JB, Cioslowski J, Stefanov BB, Nanayakkara A, Challacombe M, Peng CY, Ayala PY, Chen W, Wong MW, Andres JL, Replogle ES, Gomperts R, Martin RL, Fox DJ, Binkley JS, Defrees DJ, Baker J, Stewart JP, Head-Gordon M, Gonzalez C, Pople JA (1995) Gaussian 94, Revision C.2. Gaussian, Pittsburgh, Pa
28. Vosko SH, Wilk L, Nusair M (1980) Can J Phys 58:1200
29. Becke AD (1988) Phys Rev A 38:3098
30. Lee C, Yang W, Parr RG (1988) Phys Rev B 37:785
31. Becke AD (1993) J Chem Phys 98:5648
32. Gill PMW, Johnson BG, Pople JA (1993) Chem Phys Lett 209:506
33. Murray CW, Handy NC, Laming GJ (1993) Mol Phys 78:997
34. Handy NC, Maslen PE, Amos RD, Andrews JS, Murray CW, Laming GJ (1992) Chem Phys Lett 197:506
35. Štrajbl M, Baumruk V, Florián J (1998) J Phys Chem B 102:1314